their Table 1 classification. Continuity arguments developed for Watt linkages in Mirth and Chase (1995) can be extended to demonstrate that all linkages on a single segment must share the same circuit attributes of any single test linkage on that segment. Therefore, if a test linkage exhibits the circuit defect, the entire segment is deleted; otherwise, the entire segment is displayed.

The Burmester curves are segmented by locating the transitional linkages between Table 1 classifications. The transitional linkage between any two possible adjacent classifications occur whenever the constituent four-bar coupler curve becomes tangent to a limit circle.

An example is illustrated in Fig. 3. The coupler curve and limit circles of Stephenson III linkage inversions corresponding to three consecutive ground pivot selections are highlighted. The first selection is a type "M2" linkage. The third is a type "S." Continuity requires the existence of the transitional second selection between them, where the coupler curve becomes tangent to the outer limit circle.

The curve sectioning procedure is implemented using logic parallel to that used for both four-bar and Watt circuit rectification in Mirth and Chase (1995). The Table 1 classifications of approximately 100 trial linkages are determined at sequential locations along the Burmester curves. If the classification changes between two trials, the trial values before and after the change are used to define an interval of uncertainty containing the transitional linkage. The location of the transitional linkage is then refined with a bisection search.

The implementation is completed by testing a single linkage within each segment for the circuit defect. Note that linkages from type "S" segments have one circuit, so test linkages are not required for these segments.

Burmester curves for the external dyad typically have many more segments than their four-bar and Watt counterparts. Figure 3 illustrates a very small portion of the overall centerpoint curve for an actual problem. The "M2" and "Z" segments included on this segment have been deleted due to the circuit defect.

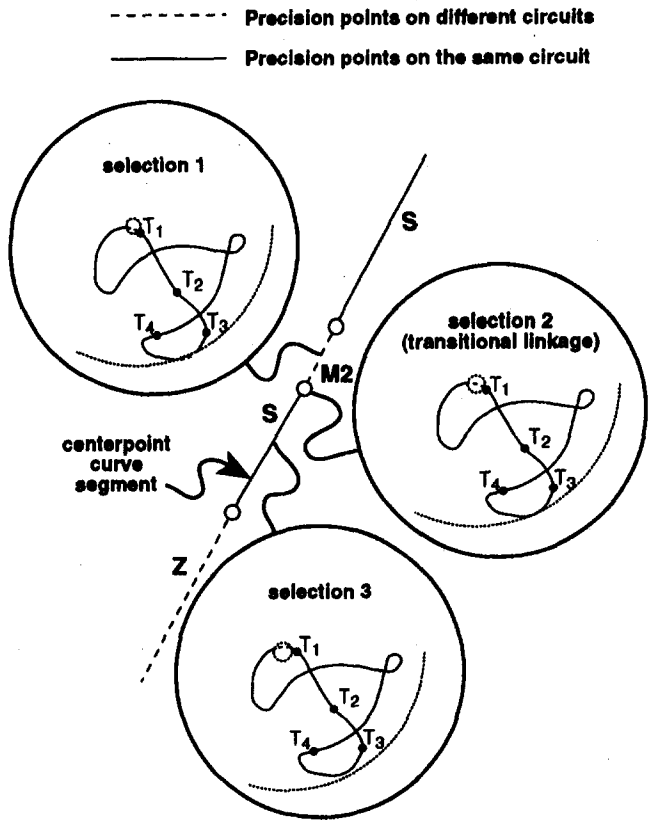

Fig. 3 Sample segment of the final centerpoint curve of a Stephenson III linkage rectified to prevent the circuit defect

Conclusion

This paper provides a method to prevent the circuit defect in any Stephenson linkage designed for four precision positions. The ability to characterize the different circuits numerically allows for the active incorporation of circuit analysis into the synthesis procedure. Combining this method with those of Mirth and Chase (1995) enables synthesizing any four-bar or six-bar linkage with a guarantee that the linkage can reach all precision positions without disassembly.

Acknowledgment

This material is based upon work supported by the National Science Foundation under Grant No. MSM-8707684. In addition, this project was partially supported by Academic Computing Services and Systems at the University of Minnesota.

References

Chase, T. R., Erdman, A. G., and Riley, D. R., 1987, "Triad Synthesis for up to Five Design Positions with Application to the Design of Arbitrary Planar Mechanisms," ASME JOURNAL OF MECHANISMS, TRANSMISSIONS, AND AUTOMATION IN DESIGN, Vol. 109, No. 4, pp. 426–434.

Chase, T. R., and Mirth, J. A., 1993, "Circuits and Branches of Single-Degree-of-Freedom Planar Linkages," ASME JOURNAL OF MECHANICAL DESIGN, Vol. 115, No. 2, pp. 223–230.

Davis, H. P., Chase, T. R., and Mirth, J. A., 1994, "Circuit Analysis of Stephenson Chain Six-Bar Mechanisms," *Mechanism Synthesis and Analysis, ASME DE-Vol. 70,* pp. 349–358.

Davis, H. P., and Chase, T. R., 1994, "Stephenson Chain Branch Analysis: Four Generic Stationary Configurations and One New Linkage Polynomial," *Mechanism Synthesis and Analysis, ASME DE-Vol. 70,* pp. 359–367.

Mirth, J. A., 1990, "Solution Rectification for the Multiple Circuit and Transmission Angle Problems in Four Position Synthesis of Six-Bar Linkages," Ph.D. Dissertation, University of Minnesota, Minneapolis, MN.

Mirth, J. A., and Chase, T. R., 1993, "Circuit Analysis of Watt Chain Six-Bar Mechanisms," ASME JOURNAL OF MECHANICAL DESIGN, Vol. 115, No. 2, pp. 214–222.

Mirth, J. A., and Chase, T. R., 1995, "Circuit Rectification for Four Precision Position Synthesis of Four-Bar and Watt Six-Bar Linkages," ASME JOURNAL OF MECHANICAL DESIGN, *in press.*

Primrose, E. J. F., Freudenstein, F., and Roth, B. 1967, "Six-Bar Motion," *Archive for Rational Mechanics and Analysis,* Vol. 24, pp. 22–77.

Watanabe, K., and Funabashi, H., 1984, "Kinematic Analysis of Stephenson's Six-Link Mechanisms (1st Report, Discrimination of Composition Loops)," *Bulletin of JSME,* Vol. 27, No. 234, pp. 2863–2870.

Watanabe, K., Huang, Z. Y., and Kawai, Y., 1987, "A Displacement Analysis of Complex Six-Link Mechanisms of the Stephenson Type," *JSME International Journal,* Vol. 30, No. 261, pp. 507–514.

White, R. J., 1987, "Solution Rectification for a Stephenson III Motion Generator," M.S. Thesis, University of Minnesota.

Planar Motion Synthesis Using an Approximate Bi-Invariant Metric

P. Larochelle[1] and J. M. McCarthy[2]

In this paper we present a technique for using a bi-invariant metric in the image space of spherical displacements for designing planar mechanisms for n (> 5) position rigid body guidance. The goal is to perform the dimensional synthesis of the mecha-

[1]Assistant Professor, Florida Institute of Technology, Melbourne, FL 32901.

[2]Professor, University of California-Irvine, Irvine, CA 92717.

Contributed by the Design Automation Committee for publication in the JOURNAL OF MECHANICAL DESIGN. Manuscript received April 1994; revised Aug. 1994. Technical Editor: B. Ravani.

nism such that the distance between the position and orientation of the guided body to each of the n goal positions is minimized. Rather than measure these distances in the plane, we introduce an approximating sphere and identify rotations which are equivalent to the planar displacements to a specified tolerance. We then measure distances between the rigid body and the goal positions using a bi-invariant metric on the image space of spherical displacements. The optimal linkage is obtained by minimizing this distance for each of the n goal positions.

1 Introduction

The notion of a metric for measuring distances between two points in a plane, or two points in space, is quite intuitive. However, a metric that measures the distance between finite positions of a rigid body (its location and orientation) is not. Furthermore, it is known that there is no distance measure which is independent of the choice of coordinate system in both the fixed and moving bodies, see Kazerounian and Rastegar (1992) and Duffy (1990). Because this distance measure is often used in the optimality criteria for linkage synthesis and robot motion planning procedures, it is undesirable to have it vary with the choice of coordinates. We address this problem by introducing spherical approximation to the desired planar positions. A bi-invariant metric exists which can be used to measure the distances between these positions. The result is a design procedure which is bi-invariant to the order of the approximating sphere. Other work in the development of bi-invariant metrics for planning spatial and planar motions have focused on bounding the volume of the moving body and are often dependent upon its shape, see Kazerounian and Rasetegar (1992).

The paper proceeds as follows. First, we approximate planar rigid body displacements with spherical displacements and show that the error induced by such an approximation is of order $1/\mathsf{R}^2$, where R is the radius of the approximating sphere. Second, we use a bi-invariant metric in the image space of spherical displacements to synthesize an optimal spherical $4R$ mechanism. Finally, we identify the planar $4R$ mechanism associated with the optimal spherical solution. The result is a planar $4R$ mechanism that has been optimized for n position rigid body guidance using an approximate bi-invariant metric with an error dependent only upon the radius of the approximating sphere. Numerical results for ten position synthesis of a planar $4R$ mechanism are presented.

2 The Image Space of Spherical Displacements

Spherical displacements are a special subset of general spatial displacements that consist of pure rotations. Spherical displacements may be represented by a 3×3 orthonormal rotation matrix which describes the orientation of the moving frame relative to the fixed frame. Associated with the matrix of rotation, $[A] = [a_{ij}]\,(i, j = 1, 2, 3)$, is an axis of rotation $\mathbf{s}$, and a rotation angle about the axis θ, which can be recovered from $[A]$ as follows,

$$\theta = \arccos\frac{a_{11} + a_{22} + a_{33} - 1}{2}$$

$$s_x = \frac{a_{32} - a_{23}}{2\sin\theta}$$

$$s_y = \frac{a_{13} - a_{31}}{2\sin\theta}$$

$$s_z = \frac{a_{21} - a_{12}}{2\sin\theta} \tag{1}$$

Using the rotation axis $\mathbf{s}$ and the angle of rotation θ we can represent a spherical displacement by the four dimensional vector $\mathbf{q}$, see Hamilton (1969), which we denote as a quaternion. The four coordinates of the quaternion, sometimes referred to as Euler parameters, are,

$$q_1 = s_x \sin\frac{\theta}{2}$$

$$q_2 = s_y \sin\frac{\theta}{2}$$

$$q_3 = s_z \sin\frac{\theta}{2}$$

$$q_4 = \cos\frac{\theta}{2} \tag{2}$$

Note that the components of the quaternion $\mathbf{q}$ satisfy the relation,

$$G_s(\mathbf{q}):\quad q_1^2 + q_2^2 + q_3^2 + q_4^2 - 1 = 0 \tag{3}$$

and lie on a unit hypersphere which we denote as *the image space of spherical displacements*.

Given two quarternions, $\mathbf{g}$ and $\mathbf{h}$, their product yields a quaternion which represents the spherical displacement obtained by the successive application of the two given displacements. We may write the product of two quarternions in the following matrix forms, see McCarthy (1990),

$$\mathbf{gh} = [g^+]\mathbf{h} = [h^-]\mathbf{g} \tag{4}$$

where,

$$[g^+] = \begin{bmatrix} -g_4 & -g_3 & g_2 & g_1 \\ g_3 & g_4 & -g_1 & g_2 \\ -g_2 & g_1 & g_4 & g_3 \\ -g_1 & -g_2 & -g_3 & g_4 \end{bmatrix}$$

and,

$$[h^-] = \begin{bmatrix} h_4 & h_3 & -h_2 & h_1 \\ -h_3 & h_4 & h_1 & h_2 \\ h_2 & -h_1 & h_4 & h_3 \\ -h_1 & -h_2 & -h_3 & h_4 \end{bmatrix}$$

3 Approximating Planar Displacements

We now examine how spherical displacements may be used to approximate planar displacements with some finite error associated with the radius R of the sphere. The approach used here is similar to the work of McCarthy (1983, 1986) in which he examined spherical and 3-spherical motions with instantaneous invariants approaching zero and showed that these motions may be identified with planar and spatial motions, respectively.

First, note that a general planar displacements, (a, b, ψ), in the $z = \mathsf{R}$ plane of a point $\mathbf{p} = (x, y)^T$ may be expressed as a coordinate transformation,

$$\begin{pmatrix} X \\ Y \\ Z \end{pmatrix} = [A_p]\begin{pmatrix} x \\ y \\ 1 \end{pmatrix} \tag{5}$$

where,

$$[A_p] = \begin{bmatrix} \cos\psi & -\sin\psi & a \\ \sin\psi & \sin\psi & b \\ 0 & 0 & \mathsf{R} \end{bmatrix} \tag{6}$$

Now consider a general spherical displacement in which the parameters used to describe the displacement are the three angles θ, ϕ, and ψ as defined in Fig. 1. We refer to θ

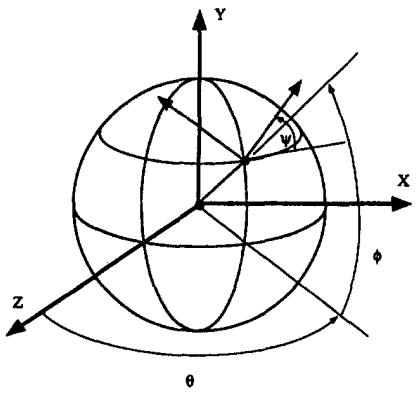

Fig. 1 Coordinates for the spherical approximation to a planar displacement

as the longitude, ϕ as the latitude, and ψ as the roll of the position. Using these parameters a general spherical displacement may be written as,

$$\begin{pmatrix} X \\ Y \\ Z \end{pmatrix} = [A_s] \begin{pmatrix} x \\ y \\ z \end{pmatrix} \tag{7}$$

where,

$$[A_s] = Rot(y, \theta) Rot(x, -\phi) Rot(z, \psi) \tag{8}$$

Performing the matrix multiplication yields,

$$[A_s] = \begin{bmatrix} \cos\theta\cos\psi - \sin\theta\sin\phi\sin\psi & -\cos\theta\sin\psi - \sin\theta\sin\phi\cos\psi & \sin\theta\cos\phi \\ \cos\phi\sin\psi & \cos\phi\cos\psi & \sin\phi \\ -\sin\theta\cos\psi - \cos\theta\sin\phi\sin\psi & \sin\theta\sin\psi - \cos\theta\sin\phi\cos\psi & \cos\theta\cos\phi \end{bmatrix} \tag{9}$$

We now define $\tilde{a}$ as the longitudinal arc length and $\tilde{b}$ as the latitudinal arc length so that, $\tilde{a} = \mathsf{R}\theta$ and $\tilde{b} = \mathsf{R}\phi$. Solving for the angles we obtain,

$$\theta = \frac{\tilde{a}}{\mathsf{R}}$$
$$\phi = \frac{\tilde{b}}{\mathsf{R}} \tag{10}$$

We now expand the trignometric functions sine and cosine using a Taylor series about 0,

$$\sin(x) = x - \frac{1}{3!}x^3 + \frac{1}{5!}x^5 - \cdots$$
$$\cos(x) = 1 - \frac{1}{2!}x^2 + \frac{1}{4!}x^4 - \cdots \tag{11}$$

Substituting the angles θ and ϕ from Eq. (10) into the expansions Eqs. (11) we are able to rewrite Eq. (9) as,

$$[A_s] = \begin{bmatrix} \cos\psi & -\sin\psi & \frac{\hat{a}}{\mathsf{R}} \\ \sin\psi & \cos\psi & \frac{\hat{b}}{\mathsf{R}} \\ 0 & 0 & 1 \end{bmatrix} + \frac{1}{\mathsf{R}} \begin{bmatrix} 0 & 0 & 0 \\ 0 & 0 & 0 \\ -\hat{a}\cos\psi - \hat{b}\sin\psi & \hat{a}\sin\psi - \hat{b}\cos\psi & -\frac{1}{2}\left(\frac{\hat{a}^2 + \hat{b}^2}{\mathsf{R}}\right) \end{bmatrix} + O\left(\frac{1}{\mathsf{R}^2}\right) \tag{12}$$

Now, if we consider only the displacement of points $\mathbf{p} = (x, y, \mathsf{R})^T$ in the $z = \mathsf{R}$ plane we may we rewrite Eq. (7) using Eq. (12) as,

$$\begin{pmatrix} X \\ Y \\ Z \end{pmatrix} = \begin{bmatrix} \cos\psi & -\sin\psi & \hat{a} \\ \sin\psi & \cos\psi & \hat{b} \\ 0 & 0 & \mathsf{R} \end{bmatrix} \begin{pmatrix} x \\ y \\ 1 \end{pmatrix} + \frac{1}{\mathsf{R}} \begin{bmatrix} 0 & 0 & 0 \\ 0 & 0 & 0 \\ -\hat{a}\cos\psi - \hat{b}\sin\psi & \hat{a}\sin\psi - \hat{b}\cos\psi & -\frac{1}{2}(\hat{a}^2 + \hat{b}^2) \end{bmatrix} \times \begin{pmatrix} x \\ y \\ 1 \end{pmatrix} + O\left(\frac{1}{\mathsf{R}^2}\right) \tag{13}$$

We note that the first term of Eq. (13) is identical to the equation for general planar displacements, Eq. (5). Moreover, in the limit as $1/\mathsf{R} \to 0$ and $(\hat{a}, \hat{b}, x, y)$ remain finite, spherical and planar motion are identical. Furthermore, we note, to the first order that the spherical motion differs from the motion in the $z = \mathsf{R}$ plane only in the z direction.

From our derivation and analysis of Eq. (13) we conclude that spherical displacements may be used to approximate planar displacements with some finite error which is associated with the radius of the sphere. The procedure used to approximate a planar displacement, (a, b, ψ), with a displacement on a sphere of radius R is as follows. Examining the first term of Eq. (13) we make the following identifications,

$$\hat{a} \Leftrightarrow a$$
$$\hat{b} \Leftrightarrow b$$
$$\psi \Leftrightarrow \psi \tag{14}$$

Finally, using the definition of the arc lengths, Eq. (10), and the radius of the sphere we obtain the three angles; θ, ϕ, and ψ, which describe the spherical displacement on the sphere of radius R that approximates the prescribed planar motion.

$$\theta = \frac{a}{\mathsf{R}}$$
$$\phi = \frac{b}{\mathsf{R}}$$
$$\psi = \psi \tag{15}$$

4 The Metric

The metric in the image space that we use was proposed by Ravani and Roth (1983) for synthesizing planar, spherical, and spatial mechanisms for rigid body guidance. Each position of a rigid body maps to a corresponding point in the image space. McCarthy (1990) shows that if the displacement is a general spatial one, the mapping is to the image space of spatial displacements, if the displacement is planar to the image space of planar displacements, and spherical displacements map to the image space of spherical displacements. Let the two image points of a rigid body displacement be denoted by $\mathbf{q}_1$ and $\mathbf{q}_2$ and let us define the vector $\mathbf{u} = (\mathbf{q}_1 - \mathbf{q}_2)$. The measure d of the distance between the two positions is defined as follows,

$$d^2 = \mathbf{u}^T\mathbf{u} = (\mathbf{q}_1 - \mathbf{q}_2)^T(\mathbf{q}_1 - \mathbf{q}_2) \tag{16}$$

We now consider a different position of the fixed reference frame described by the image space point $\mathbf{q}_F$. As viewed from the new fixed reference frame the positions are,

$$\mathbf{q}'_1 = \mathbf{q}_F\mathbf{q}_1 = [q_F^+]\mathbf{q}_1$$
$$\mathbf{q}'_2 = \mathbf{q}_F\mathbf{q}_2 = [q_F^+]\mathbf{q}_2 \tag{17}$$

Next, we compute the distance between the two positions when referenced to the fixed frame at a general position $\mathbf{q}_F$. By substituting Eq. (17) into Eq. (16) we arrive at,

$$d^2 = \mathbf{u}^T[q_F^+]^T[q_F^+]\mathbf{u} \tag{18}$$

For planar and spatial displacements, $[q_F^+]^T[q_F^+] \neq [I]$ and the metric is not invariant under a change of fixed frame coordinate system. However, in the image space of spherical displacements we have, from Eq. (3) and Eq. (4), that $[q_F^+]^T[q_F^+] = [I]$ for all $\mathbf{q}_F$, see McCarthy (1990). Therefore, the distance obtained in Eq. (18) is identical to that obtained in Eq. (16) and we see that the metric is invariant to multiplication on the left, i.e., left invariant. Similarly, suppose $\mathbf{q}_1$ and $\mathbf{q}_2$ are measured with respect to a moving frame. We now examine a change in the position of the moving frame described by the image space point $\mathbf{q}_M$. As viewed from the new moving reference frame the positions are,

$$\mathbf{q}''_1 = \mathbf{q}_1\mathbf{q}_M = [q_M^-]\mathbf{q}_1$$
$$\mathbf{q}''_2 = \mathbf{q}_2\mathbf{q}_M = [q_M^-]\mathbf{q}_2 \tag{19}$$

We compute the distance between the two positions by substituting Eq. (19) into Eq. (16) and arrive at,

$$d^2 = \mathbf{u}^T[q_M^-]^T[q_M^-]\mathbf{u} \tag{20}$$

Again, we have that $[q_M^-]^T[q_M^-] = [I]$ for all $\mathbf{q}_M$ and conclude that the metric, given by Eq. (16), in the image space of spherical displacements is both left and right invariant, or bi-invariant. That is to say, our measure of the distance between two positions in the image space of spherical displacements is independent of the choice of coordinate system used. For a more general discussion of metrics and norms see Chapter 10: Computational Kinematics, edited by K. C. Gupta in Erdman (1992).

5 The Design Procedure

First, determine the spherical positions which approximate the n desired positions of the rigid body by using Eq. (15) and Eq. (9). The next step in the procedure is to synthesize a spherical mechanism which guides a rigid body through the spherical positions which approximate the n desired positions of the moving body in the plane.

The synthesis procedure used to perform the n position spherical $4R$ rigid body guidance problem was presented by Bodduluri and McCarthy (1992), and Ravani and Roth (1983). The procedure first approximates the point on the constraint manifold of the mechanism which is closest to the desired point in the image space. The metric, given by Eq. (16), is used to measure the distance from this point on the constraint manifold to the desired point in the image space. An optimization problem is then formulated to vary the design parameters of the mechanism such that they minimize this distance for each of the n desired positions. The result is a spherical $4R$ mechanism whose design variables have been optimized such that all of the prescribed positions are either: (*1*) in the constraint manifold, or, (*2*) the constraint manifold has been shaped such that it comes as close as possible to all of the desired positions. Once the optimal spherical mechanism has been found the final step of the design process is to obtain the planar $4R$ mechanism associated with the spherical $4R$ mechanism by using Eq. (15).

Table 1 Ten planar positions (a, b, ψ), the approximating spherical positions, and the spherical design error

Pos.	a	b	ψ	Long.	Lat.	Roll	Error
1	0.0	0.0	40.0	0.000	0.000	40.000	$1.07E-5$
2	4.5	4.0	20.0	2.578	2.291	20.000	$3.36E-5$
3	8.5	8.0	0.0	4.870	4.583	0.000	$1.93E-5$
4	13.0	11.5	−30.0	7.448	6.589	−30.000	$1.01E-5$
5	13.0	12.5	−35.0	7.448	7.161	−35.000	$2.67E-5$
6	9.5	14.0	−35.0	5.443	8.021	−35.000	$3.91E-6$
7	5.0	13.5	−30.0	2.864	7.734	−30.000	$6.47E-6$
8	1.0	10.5	−15.0	0.572	6.016	−15.000	$6.14E-6$
9	−1.0	6.5	0.0	−0.572	3.724	0.000	$1.90E-5$
10	−1.5	3.0	20.0	−0.859	1.718	20.000	$1.10E-1$
							$\sum = 1.47E-4$

6 Case Study

We now present an example of the design of a planar $4R$ mechanism for $n = 10$ positions. The 10 desired positions are listed in Table 1. These are the same 10 positions that were used by Ravani and Roth (1983) to demonstrate their planar synthesis procedure. Based upon the coordinates of the desired positions we choose to limit the design space to a 52×52 square; ($4 \times 13 = 52$). That is to say we limit the mechanism search space to this planar area such that the moving and fixed axes, as well as the rigid body being guided, are always within this area. Limiting the angles θ and ϕ about the z axis to; $-15 \leq \theta \leq 15$ and $-15 \leq \phi \leq 15$, we now compute the radius of the approximating sphere,

$$\mathrm{R} = \frac{52}{30\dfrac{\pi}{180}} \approx 100 \tag{21}$$

The longitude, latitude, and roll of the spherical positions which approximate the desired planar positions are found in Table 1. Furthermore, the error measure indicating how closely the spherical $4R$ mechanism guides the body through each of the spherical positions is also listed in Table 1. The result of the spherical optimization is the location (longitude and latitude) of the fixed and moving axes of the spherical mechanism. Using Eq. (15), we obtain the locations of the planar axes which are associated with the spherical mechanism. The driving crank has its fixed axis at (13.98, −2.53) and its moving axis at (10.23, −4.66). The driven crank has its fixed axis at (6.57, 1.12) and its moving axis at (2.66, −7.84). Note that the locations of the fixed axes are given with respect to the fixed frame while the locations of the moving axes are given with respect to the moving reference frame. The length of the fixed and the coupler links are found by computing the linear distance between the fixed and moving axes, respectively. To determine the crank lengths of each dyad we use Eq. (15) to recover the linear distance between the fixed and moving axes of the planar linkage from the angular length of the corresponding spherical crank. The four link lengths of the mechanism are listed in Table 2.

Table 2 Planar link lengths obtained using the spherical approximation before and after the coordinate change

Link	Length(orig)	Length(trans)
DRIVING	6.869	6.864
COUPLER	8.204	8.204
DRIVEN	5.187	5.188
FIXED	8.267	8.277

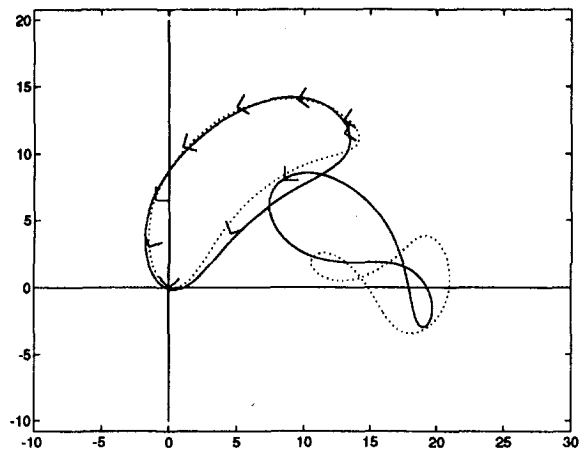

Fig. 2 Coupler curves obtained using Ravani's method (dotted) and the spherical approximation (solid)

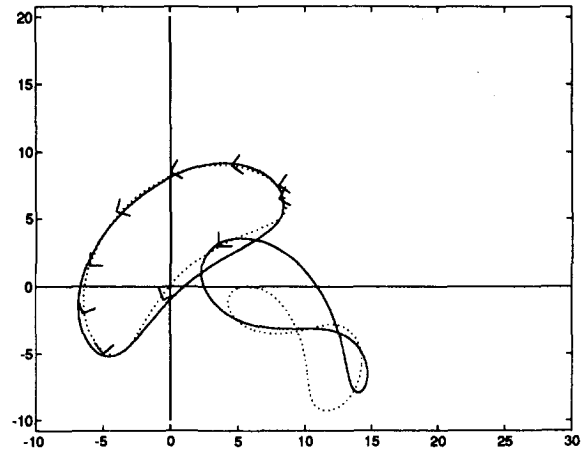

Fig. 3 Coupler curves obtained after a coordinate change: Ravani's method (dotted), the spherical approximation (solid)

In order to verify the design we use an approach presented by Suh and Radcliffe (1978) which utilizes the crank constraint equation for a planar *RR* dyad. We substitute the fixed and moving axes of the mechanism into the crank constraint equation and solve for the crank length. If the mechanism passes exactly through all of the positions then the crank length should remain constant. The results of the verification are the standard deviation of the 10 crank lengths obtained from the crank constraint equation. The standard deviations of the driving and driven crank lengths are 0.560 and 0.288, respectively. For the sake of comparison we include the results of the verification of the solution presented by Ravani and Roth (1983) to the same 10 positions using the metric given by Eq. (16) in the image space of planar displacements, which you may recall is not bi-invariant. The standard deviations of the driving and driven crank lengths for the solution presented by Ravani and Roth are 0.157 and 0.739, respectively. Note that the sum of the standard deviations for the spherical approximation solution, 0.8481, is less than that for Ravani and Roth's solution, 0.8959. The link lengths of the planar synthesis solution are listed in Table 3. The ten desired positions and the coupler curves for both the spherical approximation solution (*solid*) and the planar approximation solution (*dotted*) are shown in Fig. 2.

We now illustrate the coordinate frame dependency of Ravani and Roth's planar synthesis procedure. In Ravani and Roth (1983) the synthesis problem is reduced to minimizing the following Lagrangian function,

$$L(\mathbf{u}, \lambda) = \mathbf{u}^T\mathbf{u} + \lambda^T([J]\mathbf{u} - \mathbf{v}) \tag{22}$$

Allowing for a change of the fixed frame coordinates the new Lagrangian function becomes,

$$L(\mathbf{u}, \lambda) = \mathbf{u}^T[q_F^+]^T[q_F^+]\mathbf{u} + \lambda^T([J][q_F^+]\mathbf{u} - \mathbf{v}) \tag{23}$$

Similarly, for a change of the moving frame coordinates the Lagrangian function becomes,

$$L(\mathbf{u}, \lambda) = \mathbf{u}^T[q_M^-]^T[q_M^-]\mathbf{u} + \lambda^T([J][q_M^-]\mathbf{u} - \mathbf{v}) \tag{24}$$

Table 3 Planar link lengths obtained using Ravani's method before and after the coordinate change

Link	Length(orig)	Length(trans)
DRIVING	5.070	4.802
COUPLER	10.00	8.042
DRIVEN	8.310	7.245
FIXED	7.540	6.772

Using arguments similar to those in our discussion of the metric it is evident that the designed linkage would depend upon the choice of coordinates.

We now demonstrate the approximate bi-invariance of our approach. We translate the 10 desired positions -5.0 in both the x and y directions while maintaining their orientations and compare the results for both the planar synthesis method of Ravani and Roth and the spherical approximation method presented here. Using the spherical approximation approach we yield a solution to the translated positions which is nearly identical to the previously determined solution of the untranslated position problem. For the spherical approximation approach, the link lengths for both the original solution and the solution to the translated positions are listed in Table 2. Using the planar synthesis technique of Ravani and Roth we yield the linkage with the link lengths listed in Table 3. We note that the link lengths have changed for the planar synthesis approach but that the link lengths obtained by using the spherical approximation approach are nearly identical to those found for the original choice of coordinates. For visual comparison, in Fig. 3 we plot the coupler curves to the spherical approximation solution (*solid*) and the planar synthesis solution (*dotted*). Note that the coupler curve for the spherical approximation is the same in both Figs. 2 and 3 while the curve for the planar synthesis solution is not. Similar results were obtained for a change in coordinates of the moving frame.

7 Conclusions

In this paper we present a design technique that uses spherical displacements to approximate planar displacements so an optimality criterion can be employed that is invariant to the choice of coordinate system. We choose the radius of the approximating sphere in accordance with selected bounds on the operational space of the design. We show that the error induced by the spherical approximation of planar motions is of the order $1/\mathsf{R}^2$, where R is the radius of the sphere. Moreover, we demonstrate our technique by synthesizing a planar $4R$ mechanism for 10 precision positions and show that a coordinate transformation of -5.0 in both the x and y directions introduces a change in link lengths of less than 0.13 percent.

References

1 Bodduluri, M., and McCarthy, J. M., 1992, "Finite Position Synthesis Using the Image Curve of a Spherical Four Bar Motion," ASME JOURNAL OF MECHANICAL DESIGN, Vol. 114, March, pp. 55–60.

2 Duffy, J., 1990, "The Fallacy of Modern Hybrid Control Theory that is Based Upon 'Orthogonal Complements' of Twists and Wrench Spaces," (editorial) *Journal of Robotic Systems*, Vol. 7, No. 2, pp. 139–144.
3 Erdman, A., 1992, *The First 40 Years of Modern Kinematics*, John Wiley and Sons.
4 Hamilton, W. R., 1969, *Elements of Quarternions*, (reprinted) Chelsea Press.
5 Kazerounian, K., and Rastegar, J., 1992, "Object Norms: A Class of Coordinate and Metric Independent Norms for Displacements," *Proc. of the 1992 ASME Design Technical Conferences, Flexible Mechanisms, Dynamics, and Analysis*, DE-Vol. 47, pp. 271–275, September.
6 McCarthy, J. M., 1983, "Planar and Spherical Rigid Motion as Special Cases of Spherical and 3-Spherical Motion," ASME JOURNAL OF MECHANISMS, TRANSMISSIONS, AND AUTOMATION IN DESIGN, Vol. 105, September, pp. 569–575.
7 McCarthy, J. M., 1986, "On the Relation Between Kinematic Mappings of Planar and Spherical Displacements," ASME *Journal of Applied Mechanics*, Vol. 53, June, pp. 457–459.
8 McCarthy, J. M., 1990, *An Introduction to Theoretical Kinematics*, MIT Press.
9 Ravani, B., and Roth, B., 1983, "Motion Synthesis Using Kinematic Mappings," ASME JOURNAL OF MECHANISMS, TRANSMISSIONS, AND AUTOMATION IN DESIGN, Vol. 105, September, pp. 460–467.
10 Suh, C. H., and Radcliffe, C. W., 1978, *Kinematics and Mechanism Design*, John Wiley and Sons.

Quadri-directional Air Thrusters for Free-floating Robot Applications

N. Batsios,[1] M. Annapragada,[1] and Sunil Kumar Agrawal[2]

This paper describes the operational theory and design of a quadri-directional air thruster ("quad") for propulsion of the free-floating robot of Ohio University. In this design, the air is drawn from a central air tank and routed to four nozzles of a quad thruster via a pressure regulator, a distribution manifold, four solenoid valves, and a quad manifold. The pressure regulator is controlled by a d.c. servomotor and the solenoid valves are turned on/off using the digital output ports of the computer. The performance characteristics of this quad thruster were determined experimentally. The experimental measurement of the thrust as a function of the regulated pressure shows a good match with the data predicted by the supporting theory.

1 Introduction

Over the last two decades, a number of analytical and experimental studies have been reported on free-floating space robots [3], [1], [5]. In an effort to understand robotic assemblies in a zero gravity space environment, a free-floating robot facility is being developed at Ohio University with a dual-arm planar robot equipped with thrusters. Regulated supply of air floats the robot on a granite surface. Two quad-thrusters are mounted on the base to propel the robot with servomotor controlled pressure regulators to direct the air to the nozzles of the quad thruster.

Even though a number of aspects of the analytical work and experimental setup could be of interest to the reader, this paper addresses the aspects of design of the quadridirectional thruster. This paper is organized in the following way. The operational theory of the air thruster is outlined in Section 2. The experiment setup and the results are described in Section 3. These are followed by conclusions.

[1] Graduate Students.

[2] Associate Professor, Mechanical Systems Laboratory, Department of Mechanical Engineering, Ohio University, Athens, OH 45701.

Contributed by the Mechanisms Committee for publication in the JOURNAL OF MECHANICAL DESIGN. Manuscript received Feb. 1994; revised May 1995. Technical Editor: B. Ravani.

2 Operational Theory

Consider a reservoir (r) that discharges air through the outlet (o) of a converging nozzle into the atmosphere. For ideal gases, under the condition of isentropic flow, using continuity and conservation of energy [4], it can be shown that the ratio of the outlet and reservoir pressures is:

$$\frac{P_0}{P_r} = \frac{1}{\left[1 + \frac{\gamma - 1}{2} M^2\right]^{\gamma/\gamma - 1}} \tag{1}$$

where $P_0 = P_{atm}$, $\gamma = 1.4$ for air, and M is the Mach number of air flow at the outlet. The ratio of the outlet temperature and reservoir temperature is given by the following equation:

$$\frac{T_0}{T_r} = \frac{1}{1 + \frac{\gamma - 1}{2} M^2} \tag{2}$$

The velocity of air V_o at the outlet is $V_o = M\sqrt{\gamma R T_0}$ and the density ratio is given by

$$\frac{\rho_0}{\rho_r} = \left[\frac{T_0}{T_r}\right]^{1/\gamma - 1} \tag{3}$$

The thrust, F, generated by the air flow is

$$F = \frac{P_0 A_0 V_0^2}{R T_0} \tag{4}$$

Once the reservoir pressure is measured, the Mach number of the air flow can be computed from Eq. (1), T_0 from Eq. (2), and the thrust from Eq. (4).

The outlet velocity of the air flow from a converging nozzle never exceeds the velocity of sound. When the Mach number of air flow at the outlet becomes one, the flow is said to be choked. On substituting $M = 1$ in the above equations, we get:

$$\frac{P_0}{P_r} = \left[\frac{2}{\gamma + 1}\right]^{\gamma/\gamma - 1}, \quad \frac{T_0}{T_r} = \frac{2}{\gamma + 1}, \quad \frac{\rho_0}{\rho_r} = \left[\frac{2}{\gamma + 1}\right]^{1/\gamma - 1} \tag{5}$$

The thrust, F, generated by the air flow is

$$F = (\rho_0 V_0 A_0) V_0 = \frac{P_r A_0 V_0^2}{R T_r} \left[\frac{2}{\gamma + 1}\right]^{\gamma/\gamma - 1} \tag{6}$$

where A_0 is the area of the outlet nozzle, V_0 is the outlet velocity of the air equal to the speed of sound, and R is the universal gas constant.

Mark's Handbook [2] modifies the volumetric flow rate of air through the outlet computed in the last two paragraphs in the following way:

$$\dot{Q}_{actual} = CEY\dot{Q}_{ideal} \tag{7}$$

where C is a coefficient based on Reynold's number of the fluid flow, E is dependent on the ratio of inlet and outlet areas of the nozzle, and Y is a function of the ratio of reservoir to outlet pressure and ratio of the inlet and outlet areas of the nozzle. Hence, the outlet thrust of the nozzle according to Mark's Handbook scales the theoretical thrust by the constant CEY.

A plot of the outlet velocity as a function of reservoir pressure is shown in Fig. 1. From this plot, we observe that the velocity of the outlet air becomes a constant once the reservoir achieves a critical pressure for the choked flow. Figure 2 shows a plot of the thrust as a function of the reservoir pressure based on the operational theory for an outlet diameter of the nozzle.